





Magneto-optical Kerr effect and nuclear resonant scattering study of uni-directional anisotropy in hard-soft magnetic bilayers

Cite as: J. Appl. Phys. **126**, 043905 (2019); <https://doi.org/10.1063/1.5108920>

Submitted: 04 May 2019 . Accepted: 03 July 2019 . Published Online: 25 July 2019

Zaineb Hussain , V. Raghavendra Reddy , Olaf Leupold, Dileep Kumar, Mukul Gupta, H.-C. Wille , and Ajay Gupta 



View Online



Export Citation



CrossMark

ARTICLES YOU MAY BE INTERESTED IN

[Measurement of spin mixing conductance in \$\text{Ni}_{81}\text{Fe}_{19}/\alpha\text{-W}\$ and \$\text{Ni}_{81}\text{Fe}_{19}/\beta\text{-W}\$ heterostructures via ferromagnetic resonance](#)

Journal of Applied Physics **126**, 043902 (2019); <https://doi.org/10.1063/1.5099913>

[Influence of the conductivity on spin wave propagation in a Permalloy waveguide](#)

Journal of Applied Physics **126**, 043904 (2019); <https://doi.org/10.1063/1.5110202>

[The effects of intraparticle structure and interparticle interactions on the magnetic hysteresis loop of magnetic nanoparticles](#)

Journal of Applied Physics **126**, 043903 (2019); <https://doi.org/10.1063/1.5094180>

Journal of
Applied Physics

SPECIAL TOPIC:
Polymer-Grafted Nanoparticles

Submit Today!

AIP
Publishing

Magneto-optical Kerr effect and nuclear resonant scattering study of uni-directional anisotropy in hard-soft magnetic bilayers

Cite as: J. Appl. Phys. 126, 043905 (2019); doi: 10.1063/1.5108920

Submitted: 4 May 2019 · Accepted: 3 July 2019 ·

Published Online: 25 July 2019



Zaineb Hussain,¹ V. Raghavendra Reddy,^{1,a)} Olaf Leupold,² Dileep Kumar,¹ Mukul Gupta,¹ H.-C. Wille,²
and Ajay Gupta³

AFFILIATIONS

¹UGC-DAE Consortium for Scientific Research, University Campus, Khandwa Road, Indore 452001, India

²Deutsches Elektronen-Synchrotron—A Research Centre of the Helmholtz Association, Hamburg 22607, Germany

³Amity Center for Spintronic Materials, Amity University, Noida 201303, India

^{a)}Electronic addresses: vreddy@csr.res.in and varimalla@yahoo.com

ABSTRACT

The present work reports the unconventional exchange bias (EB) phenomena in an exchange-coupled hard and soft magnetic bilayer system and the tunability of EB. The EB phenomena, i.e., shifting of the hysteresis loop of the soft (Fe) layer is observed when the hard magnetic (Ll_0 FePt) layer is under the remanent state indicating the development of unidirectional anisotropy. The nuclear resonant scattering measurements clearly reveal the development of unidirectional anisotropy in the soft magnetic (Fe) layer, when the hard magnetic layer is under the remanent state. The magnetization reversal process is investigated by measuring two in-plane orthogonal components of magnetization, i.e., parallel (M_{\parallel}) and perpendicular (M_{\perp}) to the applied field using the magneto-optical Kerr effect (MOKE). When the magnetic field is applied parallel (antiparallel) to the biasing field direction, (H_{SAT}) magnetization reversal is nonuniform, and on the other hand, the rotation of magnetization is observed when the magnetic field is applied away from the H_{SAT} direction. In addition, the sign inversion of the M_{\perp} component is observed when the magnetic field is applied at the same angle on either side of the H_{SAT} direction, which clearly imply the change in handedness of the chirality of spin structure during the magnetization reversal of the soft layer. Further, it is observed that the EB decreases with the increase of soft magnetic (Fe) layer thickness, demonstrating the tunable nature of EB phenomena even in these unconventional systems.

Published under license by AIP Publishing. <https://doi.org/10.1063/1.5108920>

I. INTRODUCTION

Recent studies indicate that exchange bias (EB) phenomena are not only restricted to ferromagnetic-antiferromagnetic (FM-AFM) systems but can also be observed in exchange-coupled magnetic layers with different magnitudes of coercive fields such as exchange spring magnets.^{1–8} The unidirectional anisotropy can be induced in such exchange spring magnets by approaching the remanent state of the hard magnetic (HM) layer after subjecting it to a saturating field (H_{SAT}). The EB effect is observed in the minor loop of the soft magnetic (SM) layer, when the HM layer is under the remanent state. The advantages of exchange spring magnets as compared to conventional EB systems (FM-AFM) include (i) one does not need to field-cool the samples across T_N of AFM for

obtaining the EB phenomena, (ii) the EB phenomena are functional even at ambient temperatures, and (iii) the magnitude of the EB shift (H_B) can be tuned by reaching the remanent state from different H_{SAT} and also by varying the angle between the external magnetic field (H_{EXT}) and H_{SAT} .^{3,7–9} However, the role of the SM layer thickness is not specifically addressed in the context of tuning the H_B in the literature.

Even though the shifting of SM minor loops along the field axis when the HM layer is in remanence indicates the development of unidirectional anisotropy, one needs to substantiate these observations with another suitable experimental method. Coherent nuclear resonant scattering (NRS) of synchrotron radiation, the time analog of Mössbauer spectroscopy, is one of the best methods to study magnetic properties of surfaces and nanoscale structures.¹⁰

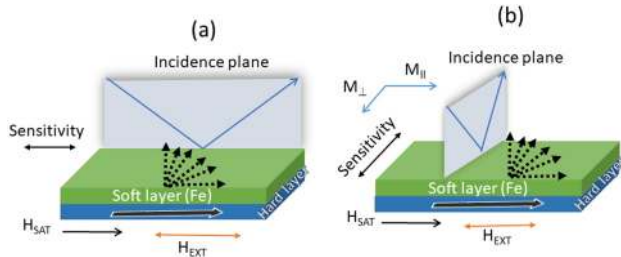


FIG. 1. (a) and (b) show the schematic of the geometries used to measure the $M_{\parallel}(H)$ and $M_{\perp}(H)$ loops. The magneto-optical (MO) sensitivity is parallel to the plane of incidence of light.

The simultaneous excitation of the hyperfine-split nuclear energy levels leads to characteristic beats in the time spectra of the nuclear decay. The analysis of the NRS beat pattern allows not only a precise determination of the magnitude of the internal hyperfine fields (H_{INT}) but also the orientation of H_{INT} in the sample. Unlike the conversion electron Mössbauer spectroscopy (energy domain) which averages out the in-plane information, the NRS measurement is also sensitive to both the in-plane azimuthal and the out-of-plane polar orientation of H_{INT} .^{10,11} It may be noted that the formation of the magnetic spiral structure in a SM film that is exchange-coupled to a HM layer (FePt/Fe) is imaged using NRS measurements.¹¹ Therefore, the measurement of H_{INT} of the SM layer with NRS would unambiguously give the information about the unidirectional anisotropy in SM/HM unconventional EB systems.

Recently, it is reported for the SM layer whose thickness is $\geq \delta$ (exchange length of the HM layer), the nucleation of the SM layer starts at a much lower field than it is proposed (which is proportional to the square of the soft layer thickness).¹³ It is because the magnetization reversal process occurs by the nonuniform process via domain nucleation and propagation rather than coherent rotation. It has also been reported that when the external magnetic field is applied along the easy-axis of magnetization, the magnetization reversal process is nonuniform for the hard/soft exchange-coupled system, whereas when applied along the hard axis, it occurs by coherent rotation.¹⁴ In order to study the magnetization

reversal process of the soft layer in such exchange spring magnets, the magneto-optical Kerr effect (MOKE) can be advantageous as it can probe both the in-plane orthogonal components of magnetization, i.e., the magnetization component which is parallel (M_{\parallel}) and perpendicular (M_{\perp}) to the H_{EXT} , respectively as shown schematically in Fig. 1.¹⁶ Therefore, one can distinguish between non-uniform magnetization reversal and coherent rotation by analyzing the angular dependent M_{\parallel} and M_{\perp} data as the coherent rotation of magnetization can give rise to significant M_{\perp} component. However, it is to be noted that it is difficult to separate M_{\parallel} and M_{\perp} precisely in conventional MOKE setup due to the oblique incidence of light and also second order effects. Therefore, the signal coming from the quadratic effect as well as from the out-of-plane component should be eliminated. The recent advances in MOKE microscopy utilizing the light from eight light emitting diode (LED) arrays makes it possible to estimate pure M_{\parallel} and M_{\perp} components.¹⁷ The contribution of the pure in-plane first order signal can be obtained by subtracting the signal of two inverted directions of oblique light incidence taken along the same axis.¹⁷

In view of the above mentioned aspects, we have studied the effects of the SM layer (Fe) thickness on the EB phenomena in the exchange spring coupled FePt/Fe bilayer system in the present work. EB is observed when such a bilayer is kept in the remanent condition of the bottom HM FePt layer. It is observed that the magnitude of the EB shift (H_B) decreases with the SM layer (Fe) thickness. MOKE and NRS measurements are used to study and confirm the induced unidirectional anisotropy at the interface of HM FePt and SM Fe layers. The present results indicate the possibility of tuning H_B and also the intricate role of the SM layer thickness in such bilayer exchange spring magnets.

II. EXPERIMENTAL

Three $L1_0$ FePt/Fe bilayers with the structure Si(sub)/Pt(5 nm)/[$L1_0$ FePt(21 nm)/Fe (\times nm)]/C(2 nm), $x = 7, 12,$ and 17 nm henceforth designated as Fe-7 nm, Fe-12 nm, and Fe-17 nm, respectively, are deposited by the DC magnetron sputtering technique. Layers of Pt ≈ 5 nm and carbon ≈ 2 nm thickness are used as buffer and capping layers, respectively. Initially, the equiatomic $Fe_{50}Pt_{50}$ film is deposited by co-sputtering Fe and Pt targets and then annealed

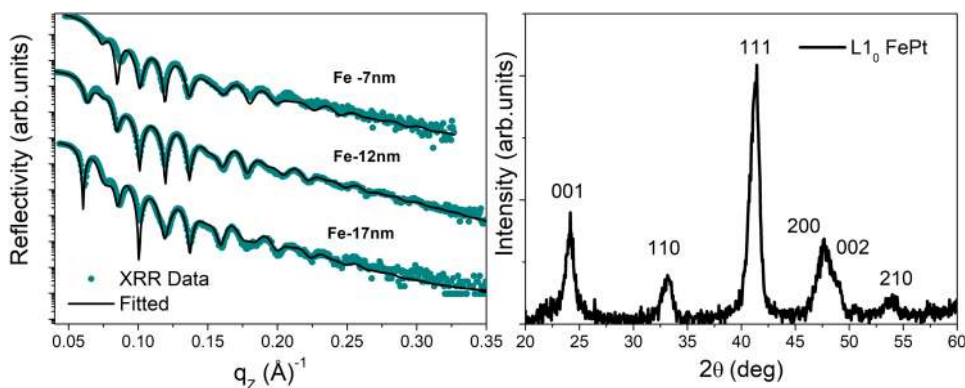


FIG. 2. (Left) X-ray reflectivity (XRR) patterns of all the films. Symbols (dark cyan) are the experimental data points, and the solid line (black) is the best fit to the data using the Parratt formalism.¹⁵ (Right) GIXRD pattern of the FePt layer, prior to the deposition of soft magnetic (Fe) layer, confirming the $L1_0$ phase formation.

TABLE I. The thickness and interface roughness as obtained from XRR pattern (Fig. 2). The typical error bar is ± 0.5 nm.

Sample	Total Fe thickness (nm)	Roughness ($\sigma_{\text{Fe-C}}$) (nm)	FePt thickness (nm)	Roughness ($\sigma_{\text{FePt-Fe}}$) (nm)
Fe-7 nm	7.1	1.9	22.4	0.9
Fe-12 nm	11.9	1.5	21.7	1
Fe-17 nm	17	1.8	21.8	1.2

in situ at 600 °C to achieve the L_{10} phase of FePt, which is confirmed with grazing incidence x-ray diffraction measured *ex situ* as shown in Fig. 2. After optimization of conditions for the preparation of the hard magnetic L_{10} FePt (21 nm) layer, the deposition of the soft magnetic (Fe) layer with different thicknesses is carried out at ambient temperatures. A probe layer of ^{57}Fe of ≈ 3 nm is introduced at the interface of FePt and Fe layers in order to do the nuclear resonance scattering (NRS) measurements. The NRS measurements are carried at P01 beam-line of DESY PETRA-III, Germany. To confirm the phase formation and for determining the thickness, grazing incidence x-ray diffraction (GIXRD) measurements with an angle of incidence of 0.5° and the x-ray reflectivity (XRR) measurements are carried out by using a Bruker D8-Discovery system equipped Cu K-radiation and LynxEye detector. The XRR patterns are analyzed by using the Parratt formalism.¹⁵ To study the exchange bias and magnetization reversal process of the SM layer, pure longitudinal and transverse MOKE measurements are performed using an advanced magneto-optical Kerr microscope (M/s Evico Magnetics, Germany) equipped with eight white LED light arrays.¹⁷ To examine the magnetization reversal process, the MOKE measurements are performed to obtain both $M_{\parallel}(H)$ and

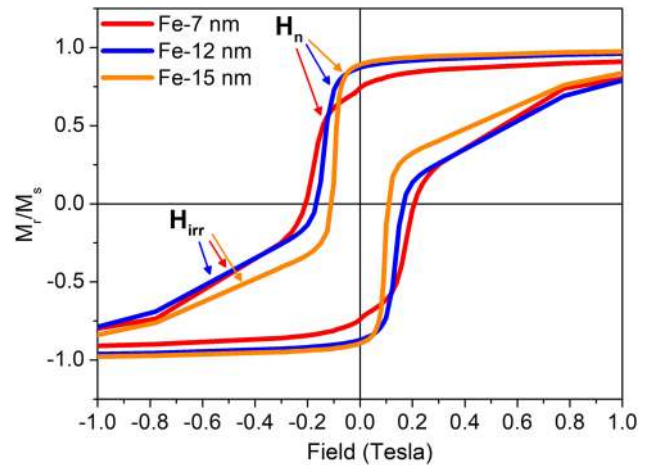


FIG. 3. Bulk M-H loops measured using a SQUID-VSM magnetometer. Nucleation field (H_n) and irreversible field (H_{irr}), which correspond to soft and hard magnetic layers, respectively, are indicated.

$M_{\perp}(H)$ loops. It is worth to mention here that M_{\perp} is sensitive to the perpendicular component of magnetization, while M_{\parallel} is sensitive to the parallel component of magnetization (M_{\parallel}) with respect to H_{EXT} as shown schematically in Figs. 1(a) and 1(b). Bulk magnetization measurements are carried out using Quantum Design SQUID-VSM.

III. RESULTS AND DISCUSSIONS

Figure 2 shows the x-ray reflectivity (XRR) data of all the bilayer samples. The XRR data are fitted with the Parratt¹⁵

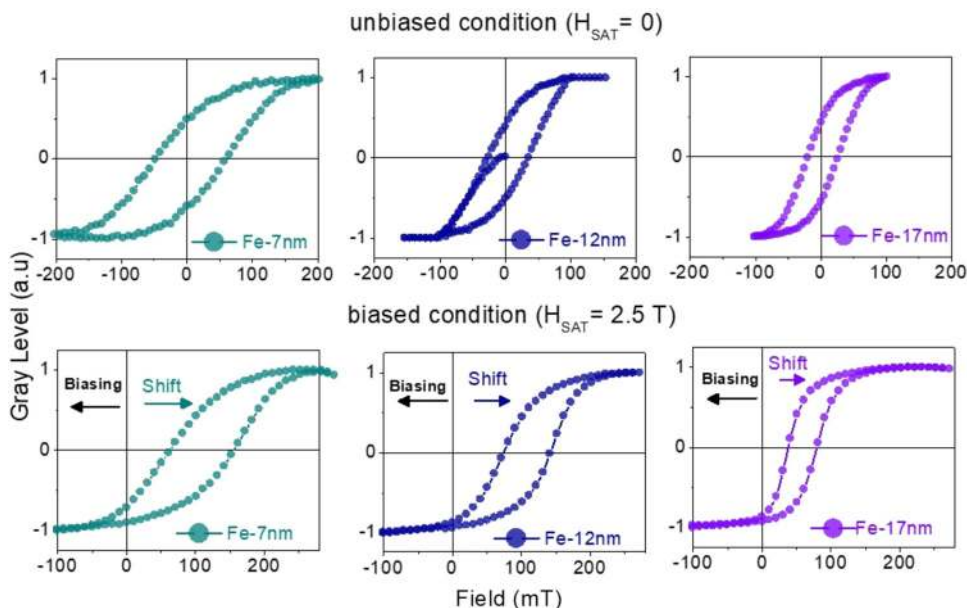


FIG. 4. Above frames show the $M_{\parallel}(H)$ loops measured in the unbiased condition ($H_{SAT} = 0$), and below frames show the $M_{\parallel}(H)$ loops measured in the biased condition ($H_{SAT} \approx 2.5$ T).

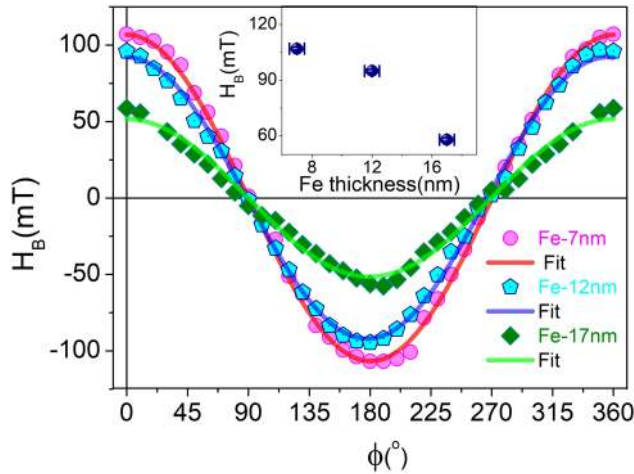


FIG. 5. Azimuthal (ϕ) variations of the exchange bias field (H_B) extracted from $M_{||}$ data (Fig. 4) measured in the biased condition ($H_{SAT} \approx 2.5$ T). Symbols are experimental data points, and the solid line is the best fit to the data using $\sum b_n \cos(n\alpha)$ as discussed in the text. The inset shows the variation of H_B corresponding to $\phi = 180^\circ$, demonstrating the tunability of H_B with the thickness of soft magnetic (Fe) layer.

formalism to get information about the thickness and the interface roughness, and the obtained values are shown in Table I. No significant variation is observed in the interface roughness as shown in Table I. Figure 2 also shows the GIXRD pattern of the 600 °C annealed FePt layer before the deposition of Fe onto it. The GIXRD data clearly show the $L1_0$ phase formation with (111) texture matching with the literature.^{7,18,19} Figure 3 shows the room temperature M-H loops of all the samples measured using the bulk magnetization measurement (SQUID-VSM) method. It is well

known that if the thickness of the SM layer is more than the exchange length (δ) of the HM layer, then the composite system is in the decoupled condition, because the SM starts to reverse at much lower fields by forming a spiral structure parallel to the interface.^{12,20} Hence, it will have two distinct switching fields, i.e., one for the SM layer which nucleates (H_n) at lower fields and another one for the HM layer which starts to switch at much higher fields (H_{irr}). While for the thinner SM layer $\leq \delta$, the composite system is in the coupled condition, because both SM and HM layers reverse together and thus have a single switching field. One can distinguish the nucleation field (H_n) which corresponds to the switching of the SM layer and the irreversible field (H_{irr}) which corresponds to the switching of the HM layer. The bulk magnetization data clearly show that for all the specimens, both the layers are decoupled. This is due to the fact that the SM layer thickness of all the bilayers is greater than δ of the HM layer [i.e., $\delta(\text{FePt}) \approx 5$ nm].²⁶

To explore the possibility of EB phenomena, the Kerr hysteresis loops are measured with the bottom HM layer in both the demagnetized and remanent states. The remanent state is achieved by subjecting the sample to a saturating magnetic field (H_{SAT}) and subsequent field reduced to zero, whereas the demagnetized state is achieved by applying an alternating field of decreasing amplitude. The remanent state is termed as biased ($H_{SAT} = 2.5$ T) and the demagnetized state as an unbiased ($H_{SAT} = 0$) condition in the present work. From Fig. 4, one can clearly observe the $M_{||}(H)$ minor loops of the SM layer under the unbiased condition is symmetrical along the field axis for all the three samples and there is an increase in the coercivity (H_C) at a lower SM layer thickness, which could be due to the effect of the bottom HM layer. Whereas a considerable shift in the opposite direction to H_{SAT} can be observed as shown in Fig. 4 in the biased condition. This indicates that the H_{SAT} aligns the HM layer moment in one direction that induce unidirectional anisotropy and, therefore, exhibits the EB phenomena similar to that of conventional FM/AFM bilayers.^{1,3,7-9} These results are similar to our previous report on the similar kind of sample,

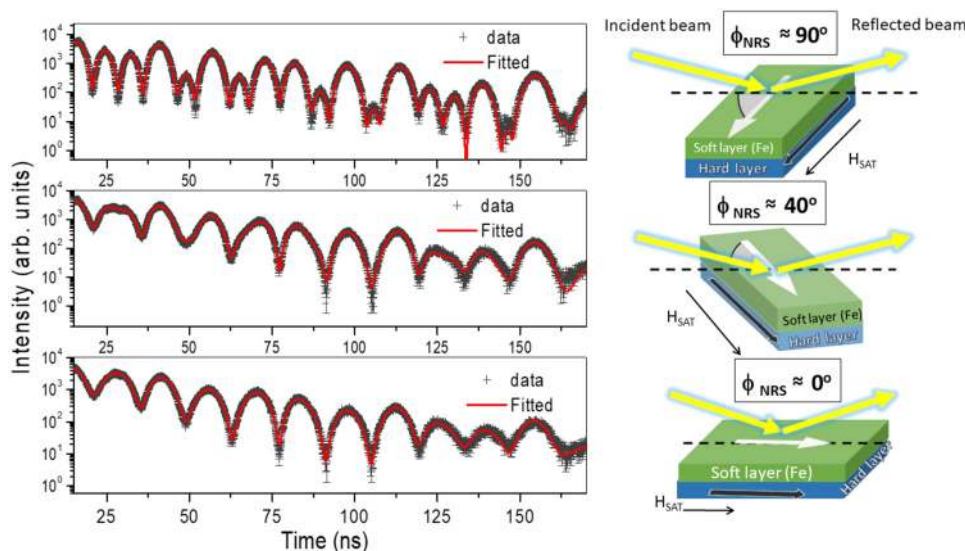


FIG. 6. Nuclear resonant scattering temporal beat patterns of the Fe-12 nm sample in the biased condition ($H_{SAT} \approx 2.5$ T) for different azimuthal orientations (ϕ_{NRS}). Symbols represent the experimental data points, and the solid line is the best fit to the data. Corresponding images on the right side panels indicate the schematic of the measurement.

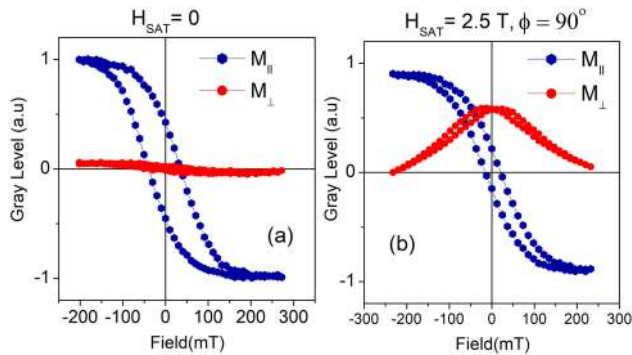


FIG. 7. (a) and (b) show the $M_{\parallel}(H)$ and $M_{\perp}(H)$ loops measured at unbiased ($H_{SAT} = 0$) and biased ($H_{SAT} = 2.5$ T) conditions at $\phi = 90^\circ$ for the Fe-12 nm sample.

however with different thicknesses of the SM layer.⁷ The inset of Fig. 5 shows the variation of H_B with the SM layer (Fe) thickness and one can clearly observe that the EB decreases with increasing thickness of the SM layer, indicating the tunable nature of EB with

the thickness of the SM layer. Further, the $M_{\parallel}(H)$ loops are measured at different azimuthal angles with respect to H_{SAT} , and the angular dependence of H_B is plotted in Fig. 5. Generally, in the conventional EB system, the angular dependence of the EB field is described by the $\sum b_n \cos(n\alpha)$, where n is a positive integer, b_n is a constant, and $\alpha = 0$ represents the direction of field cooling, n is always odd for the H_B .²⁷ In the present work also, the H_B behavior is found to follow the same conventional EB angular behavior as shown in Fig. 5.

To further confirm the development of unidirectional anisotropy, NRS measurements, time domain analog of Mössbauer spectroscopy, are performed on the biased samples ($H_{SAT} \approx 2.5$ T). The NRS measurements are carried out in zero external magnetic field. Figure 6 shows the temporal beat patterns taken for the biased Fe-12 nm sample at the selected azimuthal orientations (ϕ_{NRS} , the angle between the direction of the incident wave vector and the direction of H_{SAT}) by rotating the sample in-plane manually. Similar data are observed for the remaining two samples, i.e., Fe-7 nm and Fe-17 nm. The NRS data are fitted by using CONUSS software,^{24,25} keeping the relevant parameters, viz., internal hyperfine field (H_{INT}), isomer shift (IS), quadrupole shift (QS), magnetic texture, polar angle (θ), azimuthal angle (ϕ_{NRS}), etc., as free variables. The structural parameters of the layers (thickness, electron

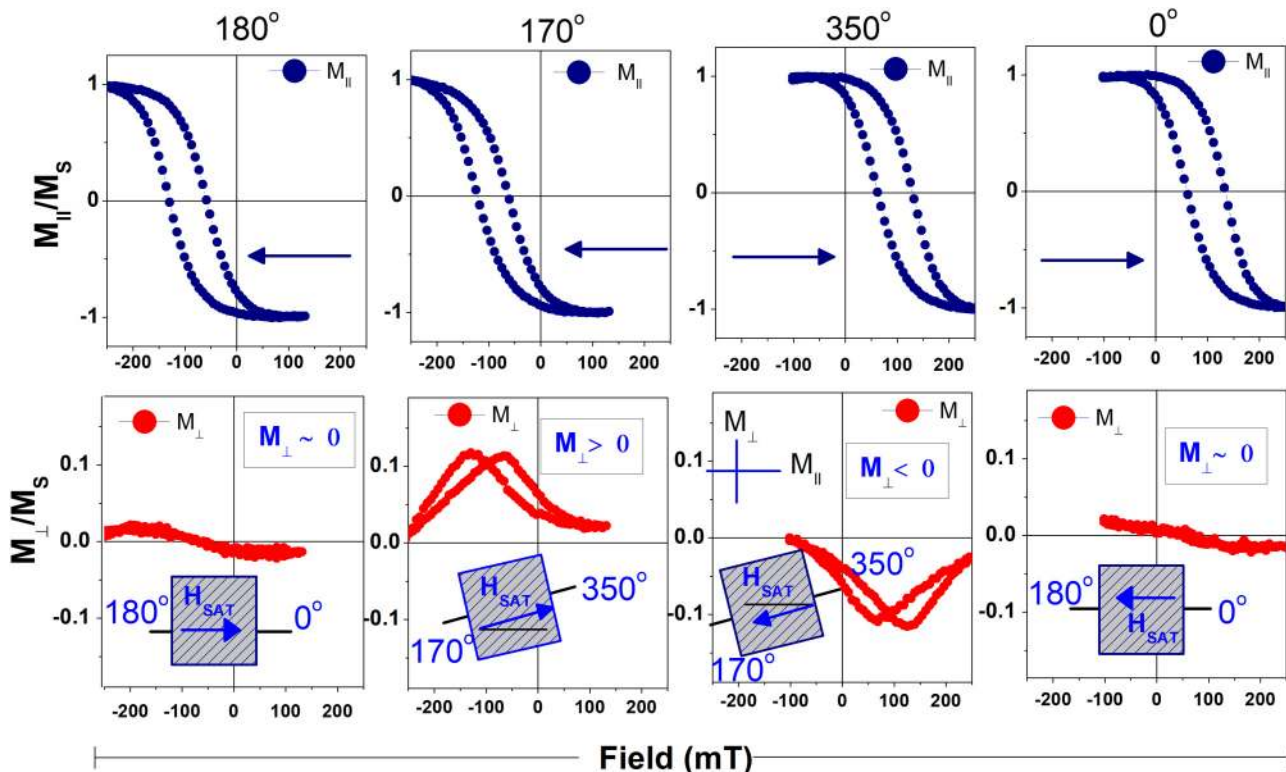


FIG. 8. $M_{\parallel}(H)$ loops (top frames) and $M_{\perp}(H)$ loops (bottom frames) measured at $\phi = 180^\circ, 170^\circ, 350^\circ,$ and 0° for the Fe-12 nm sample measured in the biased condition ($H_{SAT} = 2.5$ T). The insets of bottom frames show the schematic illustrating the angle ϕ (angle between H_{EXT} and H_{SAT}).

density, etc.) are taken from the XRR data as the input in analyzing the NRS data. Hyperfine parameters, viz., H_{INT} of 32.8 ± 0.1 T, θ of about 90° , zero IS, QS values are observed from the fitting. The obtained hyperfine parameters are consistent with the polycrystalline iron film exhibiting in-plane magnetization, as expected. However, the obtained values of ϕ_{NRS} are significantly different, viz., 87.3 ± 0.2 , 34.1 ± 0.1 , and -1.4 ± 0.1 for the three NRS patterns as shown in Fig. 6. This clearly shows that the SM layer (Fe) H_{INT} at the interface of the HM layer is along the direction of H_{SAT} in the biased condition, indicating the development of unidirectional anisotropy. Therefore, the NRS data corroborate the MOKE data as shown in Fig. 4 and clearly confirm that the composite magnetic systems consisting of HM and SM layers exhibit unidirectional anisotropy similar to that of conventional EB systems. Slight variations in the ϕ_{NRS} values could be due to the manual alignment of the sample during the NRS measurements.

Figure 7 shows the M_{\parallel} and M_{\perp} data for Fe-12 nm in unbiased ($H_{SAT} = 0$) and biased ($H_{SAT} \approx 2.5$ T) conditions. If there is an exchange spring formation of the SM layer during its reversal, it may lead to the appearance of M_{\perp} , which can be clearly distinguishable in the $M_{\perp}(H)$ loops.²⁸ However for $H_{SAT} = 0$ and a given in-plane azimuthal angle, no M_{\perp} signal is observed as shown in Fig. 7(a). No M_{\perp} signal is observed over the entire in-plane angular range (not shown). On the other hand, for the biased ($H_{SAT} \approx 2.5$ T) condition at $\phi = 90^\circ$, a large increment in M_{\perp} signal and emergence of two peaks may indicate the formation of exchange spring during the reversal of field. Gradual branches of $M_{\perp}(H)$ loops indicate that the magnetization rotation is occurring rather than nucleation of transverse or perpendicular domains which is less likely to be possible in Fig. 7(b).

To get a more deep insight into the nature of the magnetization reversal process, both $M_{\parallel}(H)$ and $M_{\perp}(H)$ loop measurements are carried out at different ϕ values for Fe-12 nm as shown in Fig. 8. One can immediately observe that at $\phi = 0^\circ$ and 180° , the M_{\perp} signal vanishes completely, indicating that the magnetization reversal process is nonuniform. Even in our previous study for thicker Fe layer ≤ 22 nm, it is evident that the fanning of moment and domain wall propagation occurred during the magnetization reversal process when the field is applied (anti) parallel to the H_{SAT} which will cause $M_{\perp} = 0$, whereas, if slightly moving away from H_{SAT} , i.e., $\phi = 170^\circ$ and 350° , the increment of the M_{\perp} signal can be observed. This indicates that a slight misalignment in the H_{EXT} and H_{SAT} can lead to changes in the reversal process into coherent rotation. Further handedness of chirality of the exchange spring can be determined by rotating the sample 180° for a given ϕ , because of the fact that the induced unidirectional anisotropy will be reversed which will give rise to the opposite chirality. The M_{\perp} signal measured at $\phi = 170^\circ$ and 350° as shown in Fig. 7 clearly demonstrates the change in handedness of chirality. This result is similar to previous reports by means of visualizing the stray magnetic fields using a magneto-optic indicator film in SmCo/Fe bilayers.^{21–23}

IV. CONCLUSIONS

In conclusion, the hard/soft exchange-coupled $L1_0$ FePt (21 nm)/Fe (7–17 nm) bilayer system in the remanent state of the hard magnetic layer (FePt) is studied with the magneto-optical

Kerr effect (MOKE) and nuclear resonant scattering (NRS). The exchange bias (EB) effect, considered to be an unconventional one, is observed in the minor loop of the soft magnetic layer when the hard layer is under the remanent state. The EB decreases with increasing soft magnetic layer thickness. The NRS measurement clearly reveals the development of unidirectional anisotropy in the soft layer, when the hard layer is under the remanent state. The formation of the exchange spring during the magnetization reversal process is investigated by two in-plane orthogonal components of magnetization, i.e., parallel (M_{\parallel}) and perpendicular (M_{\perp}) to the applied field using the magneto-optical Kerr effect (MOKE). In addition, the sign inversion of the M_{\perp} MOKE is observed on either side of the biasing direction (H_{SAT}), which clearly manifest the change in the chirality of spin structure during the reversal of the soft magnetic layer. The present results demonstrate that the combination of MOKE and NRS measurements gives unambiguous evidence for the development of unidirectional anisotropy in hard/soft magnetic layers and, therefore, is suitable to explore such unconventional EB systems. Further, it would be interesting to extend the NRS measurements, being sensitive to Mössbauer isotope only,¹¹ as a function of the external magnetic field, depth, etc., to image the spin structure of the soft magnetic (Fe) layer in such unconventional EB systems.

ACKNOWLEDGMENTS

Z.H. acknowledges CSIR, India for the fellowship in the form of SRF. Z.H. would like to thank Ms. Seema and Ms. Niti for the help during the film deposition. V.R.R. would like to acknowledge the financial support by the Department of Science and Technology (Government of India) provided within the framework of the India@DESY collaboration for the NRS measurements. V.R.R. would like to thank Dr. I. Sergueev for the help during NRS measurements. The help of Ms. Anjali Panchwane during the NRS measurements is thanked.

REFERENCES

- 1 E. E. Fullerton, J. S. Jiang, and S. D. Bader, *J. Magn. Magn. Mater.* **200**, 392 (1999).
- 2 T. Klein, K. Schlage, E. Buchholz, U. Marx, E. Burkel, and R. Rohlsberger, *New J. Phys.* **9**, 312 (2007).
- 3 S. Polisetty, S. Sahoo, A. Berger, and C. H. Binck, *Phys. Rev. B* **78**, 184426 (2008).
- 4 A. Berger, O. Hovorka, G. Friedman, and E. E. Fullerton, *Phys. Rev. B* **78**, 224407 (2008).
- 5 Ch. Binck, S. Polisetty, X. He, and A. Berger, *Phys. Rev. Lett.* **96**, 067201 (2006).
- 6 A. Berger, D. T. Margulies, and H. Do, *Appl. Phys. Lett.* **85**, 1571 (2004).
- 7 Z. Hussain, D. Kumar, V. Raghavendra Reddy, and A. Gupta, *J. Magn. Magn. Mater.* **430**, 78–84 (2017).
- 8 S. Singh, D. Kumar, B. Bhagat, R. J. Choudhary, V. R. Reddy, and A. Gupta, *J. Phys. D Appl. Phys.* **51**, 075006 (2018).
- 9 V. Alexandrakos, D. Kechrakos, N. Moutis, D. Niarchos, G. Hadjipanayis, and I. Panagiotopoulos, *J. Appl. Phys.* **119**, 123905 (2016).
- 10 R. Rohlsberger, J. Bansmann, V. Senz, K. L. Jonas, A. Bettac, K. H. Meiwes-Broer, and O. Leupold, *Phys. Rev. B* **67**, 245412 (2003).
- 11 R. Rohlsberger, H. Thomas, K. Schlage, E. Burkel, O. Leupold, and R. Ruffer, *Phys. Rev. Lett.* **89**, 237201 (2002).

- ¹²E. E. Fullerton, J. S. Jiang, M. Grimsditch, C. H. Sowers, and S. D. Bader, *Phys. Rev. B* **58**, 12193 (1998).
- ¹³A. Quesada, G. Delgado, L. Pascual, A. M. Aragón, P. Marín, C. Granados-Mirallas, M. Foerster, L. Aballe, J. E. Prieto, J. de la Figuera, J. F. Fernández, and P. Prieto, *Phys. Rev. B* **98**, 214435 (2018).
- ¹⁴S.-S. Yan, W. J. Liu, J. L. Weston, G. Zangari, and J. A. Barnard, *Phys. Rev. B* **63**, 174415 (2001).
- ¹⁵L. G. Parratt, *Phys. Rev.* **95**, 359 (1954).
- ¹⁶J. McCord, *J. Phys. D Appl. Phys.* **48**, 333001 (2015).
- ¹⁷I. V. Soldatov and R. Schafer, *Rev. Sci. Instrum.* **88**, 073701 (2017).
- ¹⁸V. R. Reddy, O. Crisan, A. Gupta, A. Banerjee, and V. Kuncser, *Thin Solid Films* **520**, 2184 (2012).
- ¹⁹V. Raghavendra Reddy, S. Kavita, and A. Gupta, *J. Appl. Phys.* **99**, 113906 (2006).
- ²⁰E. F. Kneller and R. Hawig, *IEEE Trans. Magn.* **27**, 4 (1991).
- ²¹V. S. Gornakov, V. I. Nikitenko, A. J. Shapiro, R. D. Shull, J. Samuel Jiang, and S. D. Bader, *J. Magn. Magn. Mater.* **246**, 80 (2002).
- ²²V. S. Gornakov, Yu. P. Kabanov, V. I. Nikitenko, O. A. Tikhomirov, A. J. Shapiro, and R. D. Shull, *J. Exp. Theor. Phys.* **99**, 602 (2004).
- ²³R. D. Shull, A. J. Shapiro, V. S. Gornakov, V. I. Nikitenko, J. S. Jiang, H. Kaper, G. Leaf, and S. D. Bader, *IEEE Trans. Magn.* **37**, 2576 (2001).
- ²⁴W. Sturhahn, *Hyperfine Interact.* **125**, 149 (2000).
- ²⁵See <http://www.nrixs.com> for “NRIXS Scientific Software.”
- ²⁶Y. H. Li, D. F. Zeng, H. J. Zhao, B. Du, J. Wei, S. Yoshimura, H. Saito, and G. Q. Li, *IEEE Trans. Magn.* **51** (11), 4800503 (2015).
- ²⁷S. P. Hao, Y. X. Suib, R. Shana, L. Sunc, and S. M. Zhou, *Thin Solid Films* **485**, 212 (2005).
- ²⁸D. Chumakov, R. Schäfer, D. Elefant, D. Eckert, L. Schultz, S. S. Yan, and J. A. Barnard, *Phys. Rev. B* **66**, 134409 (2002).